A Model of Blood–Brain Barrier Permeability to Water: Accounting for Blood Inflow and Longitudinal Relaxation Effects

Emmanuel L. Barbier,[1,2]* Keith S. St. Lawrence,[3] Emmanuelle Grillon,[1] Alan P. Koretsky,[2] and Michel Décorps[1]

A noninvasive technique for measuring the permeability of the blood–brain barrier (BBB) to water could help to evaluate changes in the functional integrity of the BBB that occur in different pathologies, such as multiple sclerosis or growth of brain tumor. Recently, Schwarzbauer et al. (Magn Reson Med 1997;37:769–777) proposed an MR method to measure this permeability based on the T_1 reductions induced by injecting various doses of paramagnetic contrast agent. However, this method may be difficult to implement in a clinical environment. Described here is a two-point technique, in which a spatially selective inversion is used to measure T_1 prior to and after injection of an intravascular contrast agent. Measurements made in the rat brain are compared to numerical simulations generated with a physiological model that accounts for blood flow and includes two different blood volumes: nonexchanging and exchanging blood volumes. Our results suggest that BBB permeability could be evaluated from the change in T_1 caused by the vascular contrast agent. This technique might provide an approach for monitoring changes in BBB permeability to water in clinical studies. Magn Reson Med 47:1100–1109, 2002.

Key words: contrast agent; cerebral blood flow; cerebral blood volume; blood-brain barrier; permeability; water

The blood–brain barrier (BBB) permeability is a valuable physiological parameter for characterizing the development of brain pathologies such as tumors (1–3), multiple sclerosis lesions (4), or stroke (5). Tofts and Kermode (1) first demonstrated that BBB permeability to molecules like gadopentetate dimeglumine could be measured with MRI. Recently, it has been observed that, in the context of brain tumors (6) or brain edema (7), earlier opening of the BBB could be detected with smaller molecules. These results suggest that the characterization of BBB permeability to molecules like gadopentetate dimeglumine (molecular weight: 938 g/mol) may not reveal early changes in the state of the BBB. Earlier changes of the BBB functional integrity could be characterized by measuring BBB permeability to smaller molecules, such as water (molecular weight: 18 g/mol) (8). Recently, Schwarzbauer et al. (9) proposed a new MRI method to measure the permeability of the BBB to water. This very efficient method is based on the measurement of the T_1 reduction of brain water as a function of the injected dose of contrast agent.

In a clinical environment, multiple injections of a contrast agent may be problematic as the maximum dose can be quickly reached and multiple T_1 measurements may be difficult to achieve within the time frame of a clinical exam. Interestingly, blood volume maps can be produced with a two-point technique using an iron oxide contrast agent (10). Therefore, it would be of interest to have a two-point method for estimating BBB permeability as well. Moreover, to suppress the effects of blood flow on the T_1 measurement, Schwarzbauer et al. (9) used a nonselective inversion. However, achieving repeated nonselective inversions in clinical applications is limited by RF deposition, especially at high magnetic fields. It would therefore be of interest to develop a method that does not require nonselective inversion for the T_1 measurement and can be performed quickly so that it could be more readily used in clinical studies.

In this work, we present a method in which T_1 measurements obtained in the absence and in the presence of a vascular contrast agent are compared. This two-point technique also uses a spatially selective inversion. Consequently, the model used in the data analysis accounts for the effect of blood flow on T_1, for flow-related changes in the apparent T_1 are the basis of arterial spin labeling techniques (11,12) and are also used in MR angiography (13). In the model proposed by Schwarzbauer et al., the entire blood volume is assumed to exchange with the tissue. The model proposed here also accounts for the limited fraction of the blood volume that exchanges water with the surrounding tissue (14). This approach suggests that with a two-point acquisition scheme and an appropriate model of analysis, the permeability – surface area product (PS) for water exchange across the BBB can be estimated.

MATERIALS AND METHODS

Animal Preparation

Six male Sprague-Dawley rats (256 ± 26 g) were anesthetized using 5% isoflurane in air enriched with 40% O_2. The isoflurane concentration was reduced to 2.5% during surgery. A femoral vein and a femoral artery were both catheterized. The vein was used to inject the contrast agent and the artery to collect blood samples. After surgery, the isoflurane concentration was reduced to 1.5% and rats were placed on a thermostated water pad. Body temperature was monitored during the experiment using a rectal probe.

[1]INSERM U438, RMN Bioclinique, Grenoble, France.
[2]Laboratory of Functional and Molecular Imaging, National Institute of Neuronal Disorders and Stroke, National Institutes of Health, Bethesda, Maryland.
[3]Laboratory of Diagnostic Radiology Research, Clinical Center, National Institutes of Health, Bethesda, Maryland.
Grant sponsor: NINDS intramural research program.
*Correspondence to: Emmanuel Barbier, INSERM U438, RMN Bioclinique, CHU Michallon – Pavillon B, 38043 Grenoble cedex 9, France. E-mail: emmanuel.barbier@ujf-grenoble.fr
Received 25 January 2001; revised 29 November 2001; accepted 24 January 2002.
DOI 10.1002/mrm.10158
Published online in Wiley InterScience (www.interscience.wiley.com).

During the entire experiment, three blood samples (0.2 ml each) were withdrawn for blood gas analysis to ensure that the animal was normocapnic and physiologically stable. Animals were sacrificed by an IA injection of chloralhydrate.

Contrast Agent

The contrast agent, Sinerem® (Guerbet Laboratories, Aulnay-Sous-Bois, France), is composed of ultrasmall superparamagnetic iron particles coated with dextran; 200 μmol of iron per kilogram of body weight (i.e., ~11.2 mg/kg) were injected IV. At this dose, the half-life of Sinerem® is about 4.5 hr (15).

MR Imaging Methods

Experiments were conducted on a 7 T magnet with actively shielded gradients (12 cm inner diameter, capable of 210 $mT.cm^{-1}$) controlled by an SMIS console. A surface coil (2.5 cm diameter single loop) for both excitation and reception of the MR signal was placed on the top of the rat's head.

A 2-mm thick coronal slice was imaged with a field of view of 40 × 40 mm^2 using a FLASH sequence (TE/TR = 2.4/4.2 ms, flip angle = 5°, matrix 64 × 64) (16). Imaging was preceded by an inversion-recovery preparation period using an adiabatic 180° pulse and 19 inversion delays (TI) in random order (10500, 28, 1926, 53, 104, 77, 241, 64, 137, 180, 89, 1466, 157, 345, 8477, 3684, 1109, 794, and 2575 ms). Because the adiabatic inversion pulse was applied with a surface coil, only a limited region of brain tissue was inverted (~1.5 cm thick, data not shown), yielding a spatially selective inversion. The repetition time was 11.0 sec and the entire sequence was repeated six times for averaging purposes (duration = 20 min). Moreover, a flow-weighted gradient-echo image of the same slice was acquired (TE/TR = 4/60 ms, flip angle = 90°, matrix 256 × 256, eight averages). Inversion-recovery and gradient-echo imaging were performed prior to and after contrast agent injection. The entire sequence of TI was repeated 17 times after injection of contrast agent to compensate for possible loss of signal due to local susceptibility effects (duration = 59 min).

Image Analysis

Data were processed using Matlab (MathWorks, Natick, MA). Images from the FLASH sequence were interpolated by zero-filling to a 256 × 256 matrix. Images acquired at the same TIs were averaged together and the inversion recovery signals, S, were fitted on a voxel-by-voxel basis to

$$\mathbf{S(TI)} = |\mathbf{M^0}(1 - 2\mathbf{C}\ \mathbf{exp}(-\mathbf{TI}/\mathbf{T}_{1,\mathrm{voxel}}))|, \qquad [1]$$

where M^0, C, and $T_{1,\mathrm{voxel}}$ were the fitted parameters. C was included to account for imperfect inversion pulses. For each of the six rats, the brain T_1 was measured by manually drawing a region of interest (ROI) on the cortex.

Blood T_1 and T_2^*

Prior to the start of the experiment, a 0.5 ml arterial blood sample was collected in a heparinized tube that was placed on the top of the rat's head. For each of the six rats, the blood T_1 in the absence of contrast agent was measured in an ROI located on the blood sample. However, the blood T_1 measurement was only based on the first repetition of the inversion-recovery time course to avoid the effects of blood cells separating from plasma and of the blood cooling.

For two rats, a 0.5 ml arterial blood sample was withdrawn at the end of the experiment in order to measure blood T_1 and T_2 in the presence of contrast agent. A saturation recovery experiment was performed on the blood sample with the same surface coil as for imaging but using hard 90° pulses (100 μs duration). The 20 delays between successive 90° pulses ranged between 25 μs and 800 ms. Assuming a good magnetic field homogeneity within the blood sample, the blood T_2^* in the presence of contrast agent was obtained from the fit of the FID with a monoexponential decay.

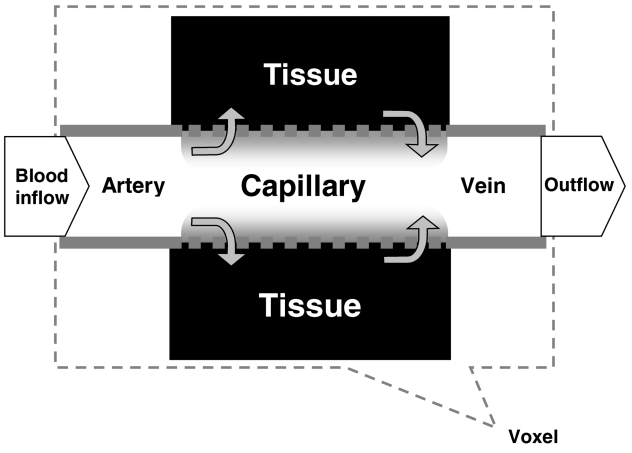

FIG. 1. Physiological model. The voxel contains blood and tissue separated by the blood–brain barrier (BBB), represented as a dotted, thick gray line. Blood flows into the voxel through arterioles and flows out of the voxel through venules. In arteries and in veins there is no exchange of water between blood and tissue. The tissue compartment is therefore only represented around the capillary compartment.

Simulation of the Physiological Model

A modified version of the model proposed by Schwarzbauer et al. (9) was used to model blood and tissue longitudinal relaxations, accounting for blood inflow and water exchange. This model, illustrated by Fig. 1, is further described in the Appendix (17). The evolution of both tissue and blood magnetizations were considered as a function of time and position (Eq. [A1]). Moreover, the blood volume was divided into three compartments: artery, capillary, and vein. Water exchange only occurred between capillaries and tissue, but not between artery and tissue or vein and tissue (Fig. 1).

In order to generate theoretical T_1 data for blood, tissue, and the total voxel compartments, the inversion-recovery was simulated using Matlab (MathWorks). The inversion was assumed to be selective, since the blood transit times from the edge of the inverted region to the edge of the imaged slice can be considered very small (<~150 ms,

(18)). Figure 2 shows an example of the evolution of the blood magnetization in both the spatial and temporal dimensions. After inversion (t = 0), the blood magnetization is $-M_b^0$ in the three compartments (artery, capillary, and vein). The effect of blood flow (arrival of uninverted magnetization), T_1 relaxation, and exchange of water between the blood and tissue compartments are taken into account, as described by Eq. [A1]. The time courses of blood and tissue signals were subsequently obtained from numerical integration of the magnetizations over the spatial dimension (Eq. [A2]). Figure 3 shows an example of the blood and tissue magnetizations obtained by such an integration. Additionally, the recovery of static, nonexchanging, blood magnetization is also presented in the figure. Finally, the apparent blood and voxel (i.e., blood + tissue) T_1 were obtained from a least-squares fit of the signal recovery to Eq. [1]. The series of inversion times, TI, used in the simulation was the same as that used in the experiments. Simulations were conducted for a blood flow of 140 ml / 100 g/min and three total blood volume fractions, V_b, of 3.0, 3.5, and 4.0% (fractions subsequently noted as V_b = 3.5@0.5%) in order to evaluate the sensitivity of the model to the blood volume (19). According to the central volume principle (20), these values yielded a mean transit time of 1.5@0.2 sec (i.e., 1.3, 1.5, and 1.7 sec, respectively, for the three different values of V_b). The arterial blood volume fraction was assumed to be 25% of the total blood volume (21,22), the capillary blood volume fraction 40% of the total blood volume (14), and the venous blood volume fraction was the remaining 35% of the total blood volume.

Simulations were performed for the conditions of contrast agent absent and present in the vasculature. The tissue T_1 was 1.84 sec; the blood T_1 was 2.3 sec in the absence of contrast agent and 0.18 sec in the presence of contrast agent (values measured at 7 T, see the Results section). The two effects of the contrast agent on blood relaxivity were accounted for as follows: to account for the short blood T_2 in the presence of contrast agent, the blood contribution in Eq. [A2] was set to zero and to account for the blood T_1 reduction, the blood T_1 measured in the presence of contrast was used in the simulations.

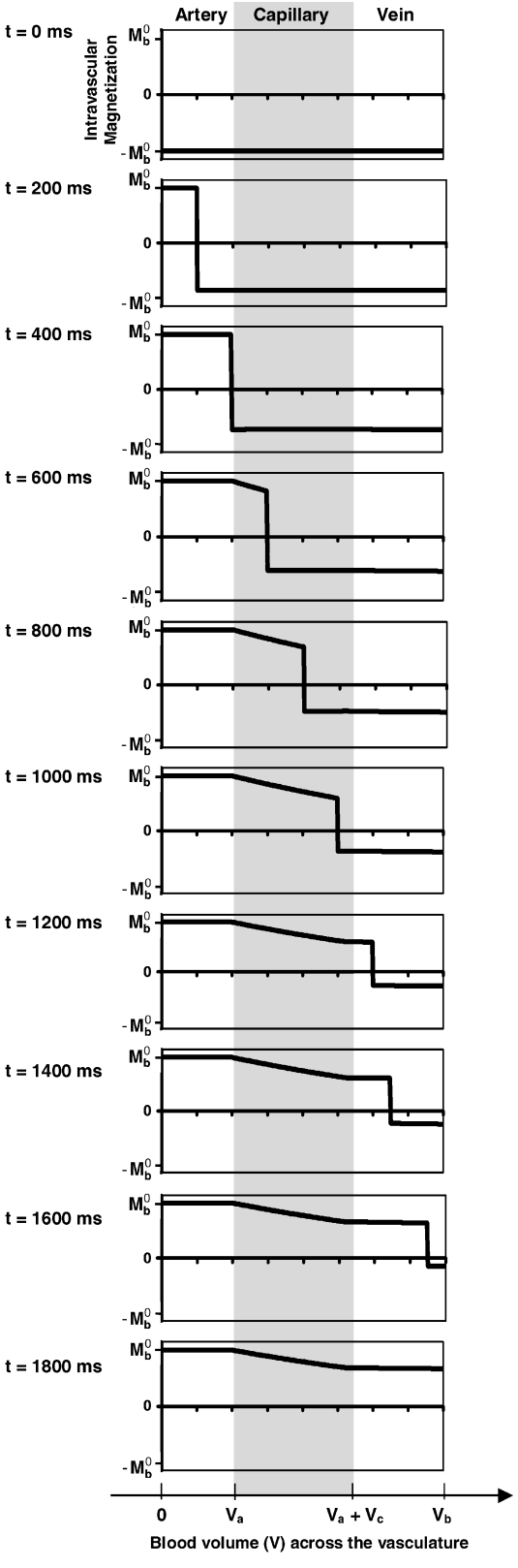

FIG. 2. Evolution of the blood magnetization in the spatial and temporal directions. Subfigures represent the blood magnetization across the spatial dimension at increasing times after the inversion pulse. The shaded area delineates the capillary compartment, surrounded by the arterial and venous compartments. The blood flow induces a constant arrival of fresh uninverted magnetization. Simultaneously, the blood magnetization relaxes, according to its T_1. This effect can be most clearly seen in the venous compartment. Finally, in the capillary compartment the exchange of water between blood and tissue is also taken into account. The parameters used for this simulation are: f = 160 ml / 100 g/min, PS = 160 ml / 100 g/min, T_{1t} = 1.84 sec, T_{1b} = 2.3 sec, total blood volume fraction = 3.5%, V_a:V_c:V_v = 25:40:35, λ = 90 ml/ 100 g.

RESULTS

All results are expressed as mean ± standard deviation.

Blood Signal

In the absence of contrast agent, the measured blood T_1 was 2304 ± 108 ms. The values of blood T_1 and T_2^* in the presence of contrast agent were 177 ± 4 ms and 0.85 ± 0.08 ms, respectively. Since the blood samples were with-

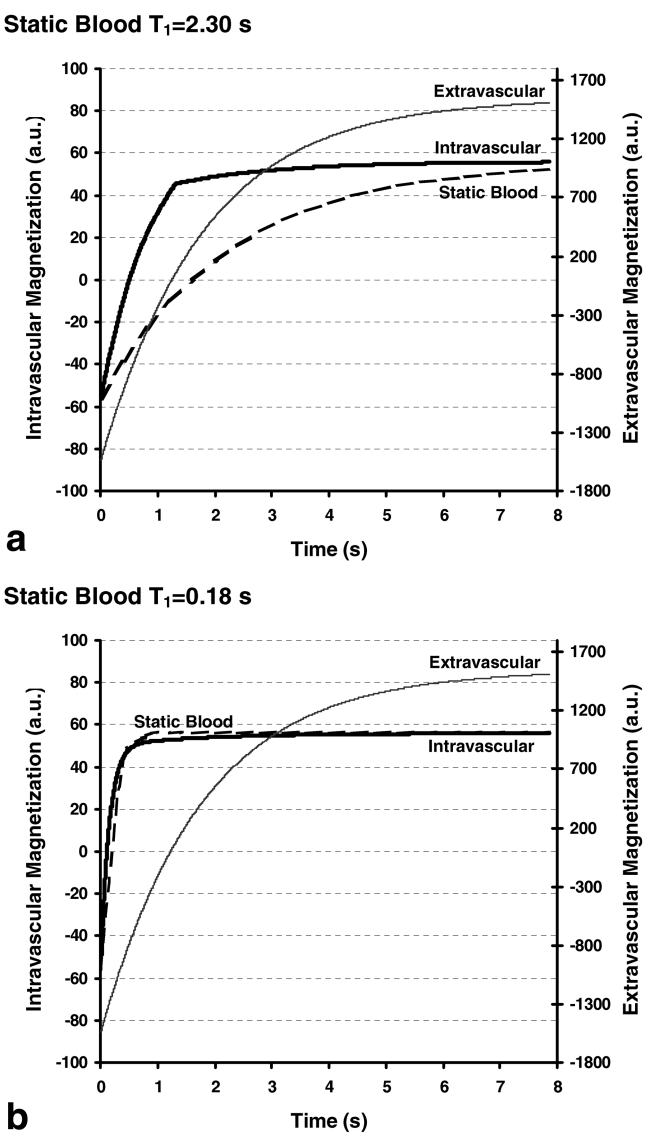

FIG. 3. Blood and tissue magnetization obtained by the integration over the spatial dimension (cf. Fig. 2) of the magnetizations computed with Eq. [A1] and static, unexchanging, blood monoexponential longitudinal relaxation (Eq. [1]). **a:** The static blood T_1 is 2.3 sec and its relaxation is represented by the dotted line. Note that the behavior of the intravascular magnetization is not exponential. **b:** The static blood T_1 is now 0.18 sec and its relaxation is represented by the dotted line. The behavior of the intravascular magnetization, as a simulation by the physiological model, is close to the static blood monoexponential relaxation. The parameters used for this simulation, except for the indicated blood T_1, are the same as that used in Fig. 2.

drawn at the end of the experiment and thus after some clearance of the contrast agent, these T_1 and T_2^* values could be overestimated. In the absence of contrast agent and at 7.0 T, Brooks et al. (23) reported blood T_2^* values between 2.7 and 10.6 ms, and Ogawa et al. (24,25) blood T_2^* values between 4 and 50 ms, depending on the oxygenation level and the hematocrit fraction. Therefore, even accounting for the contrast agent clearance and considering the FLASH sequence echo time (2.4 ms), this implies that less than 9% of the original blood signal contributed to the MR signal after contrast agent injection. The estimated reduction of contrast agent concentration at the end of the data acquisition can be estimated around 20%. This implies that there is a slight difference between the conditions in which the T_1 maps were acquired (17 averages over 1 hr) and the blood T_1, measured at the end of the experiment (i.e., 1 hr after injection).

Figure 4a,b shows the gradient echo images of the rat brain obtained before and after injection of contrast agent. Due to inflow effects, the blood vessels are clearly visible before injection. In contrast, the blood vessels are no longer visible after injection (Fig. 4b), such as the sinus vein. Considering the echo time of the flow-weighted, gradient-echo, sequence (4 ms), this is in good agreement with the blood T_2^* measured in the presence of contrast agent.

T_1 Mapping

Figure 5a,b shows the T_1 maps obtained before and after injection of the contrast agent. The only readily visible reduction in T_1 occurred in the temporal muscle. Figure 5c represents $(T_{1,\text{before}} - T_{1,\text{after}})/T_{1,\text{before}}$. A decrease in voxel T_1 can be observed throughout the brain, except in a few small regions located below the cortex, as indicated by the arrows in Fig. 5c. The regions where the voxel T_1 increased were observed in all six rats and their extent (before zero-filling) did not exceed 1 or 2 contiguous voxels ($\sim 0.6 \times 1.2 \times 2.0$ mm^3). Figure 5d shows an angiogram obtained by subtracting the image in Fig. 4b from the image in Fig. 4a. Blood vessels and regions with a high blood volume appear in white.

For all the animals, the brain cortex T_1 was 1773 $\pm$ 67 ms before injection of contrast agent and 1709 $\pm$ 39 ms after injection of contrast agent. The reduction in the brain cortex T_1 was 3.6 $\pm$ 1.6%, which was statistically significant (paired t-test, $P < 0.01$).

Figure 6 shows the time courses of two voxels in the imaging slice. The values of the parameters obtained by fitting Eq. [1] to the data points are presented in Table 1. Figure 6a shows a voxel taken in the cortex; an $\sim$6% reduction of its T_1 and a $\sim$9% reduction of M^o can be observed. The M^o reduction is due to both the dramatic decrease of the blood T_2^* and the susceptibility effect in the tissue. Figure 6b shows the time course of a voxel in which the T_1 increased by about 14% after injection of contrast agent. Note also that M^o for this voxel is barely reduced in presence of contrast agent. This lack of an effect on M^o suggests that the blood volume in the voxel is small.

Simulations Based on the Physiological Model

Figure 7 shows the apparent voxel T_1 obtained from numerical simulations of the physiological model. Figure 7a shows simulations of the apparent voxel T_1 as a function of the PS product in the absence and presence of contrast agent in the vasculature. For low BBB permeabilities to water (PS $<$ $\sim$140 ml / 100 g/min), the simulation predicts that the apparent voxel T_1 after injection of contrast agent will be larger than the apparent voxel T_1 prior to the injection of contrast agent. This could correspond to the

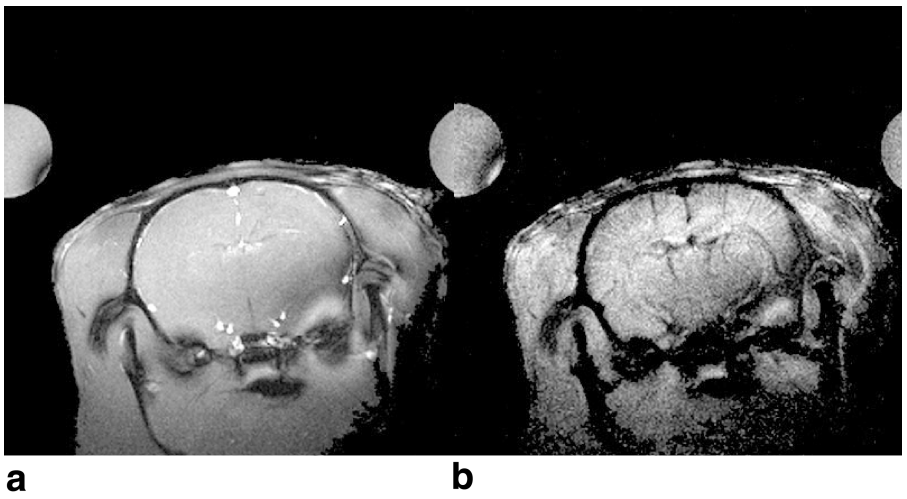

FIG. 4. Coronal, flow-weighted, gradient-echo images at 7 T of the rat brain in absence (**a**) and in the presence (**b**) of contrast agent. In a field of view of 40 mm, the in-plane resolution is 155 × 155 μm^2 and the slice thickness is 2 mm. In **b**, one can observe that the blood signal has totally disappeared in arteries as in veins.

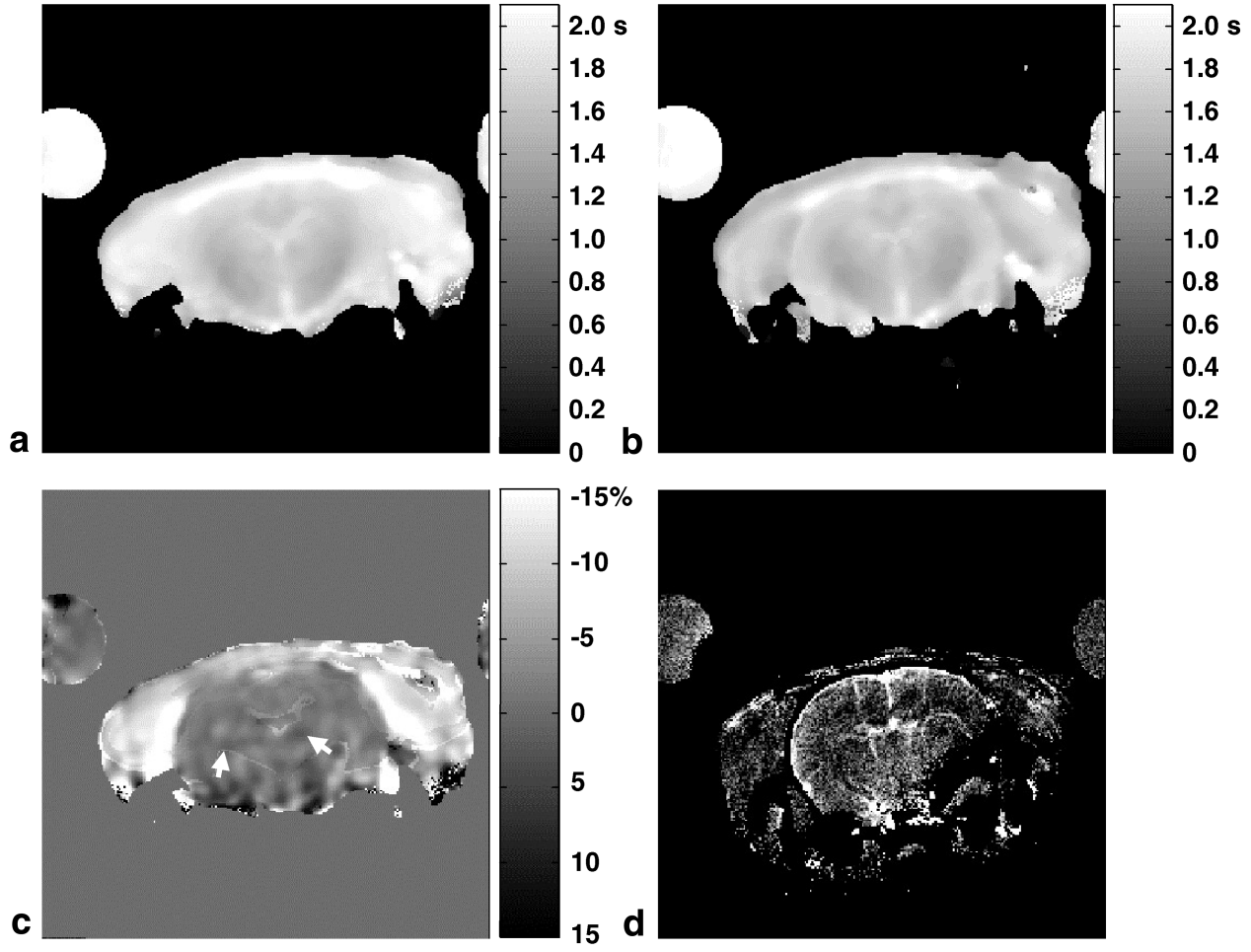

FIG. 5. Coronal maps computed from the data acquired on a single rat at 7 T. T_1 maps of the rat brain obtained before (**a**) and after (**b**) injection of a high dose of an intravascular contrast agent. **c:** Relative change in T_1 due to contrast agent injection [(image **a**)−(image **b**)]/(image **a**)*100. White (negative values) represents a decrease in T_1. **d:** Difference between angiograms acquired before and after injection of contrast agent, computed as in **c**. Because of the blood T_2^* reduction in presence of contrast agent, the blood vessels appear in white. For maps **a–c**, the field of view is 40 mm; acquisition in-plane resolution is 625 × 625 μm^2 and the slice thickness 2 mm (after zero-filling, the in-plane resolution is 155 × 155 μm^2). For map **d**, the field of view is 40 mm; acquisition in-plane resolution: 155 × 155 μm^2; slice thickness 2 mm.

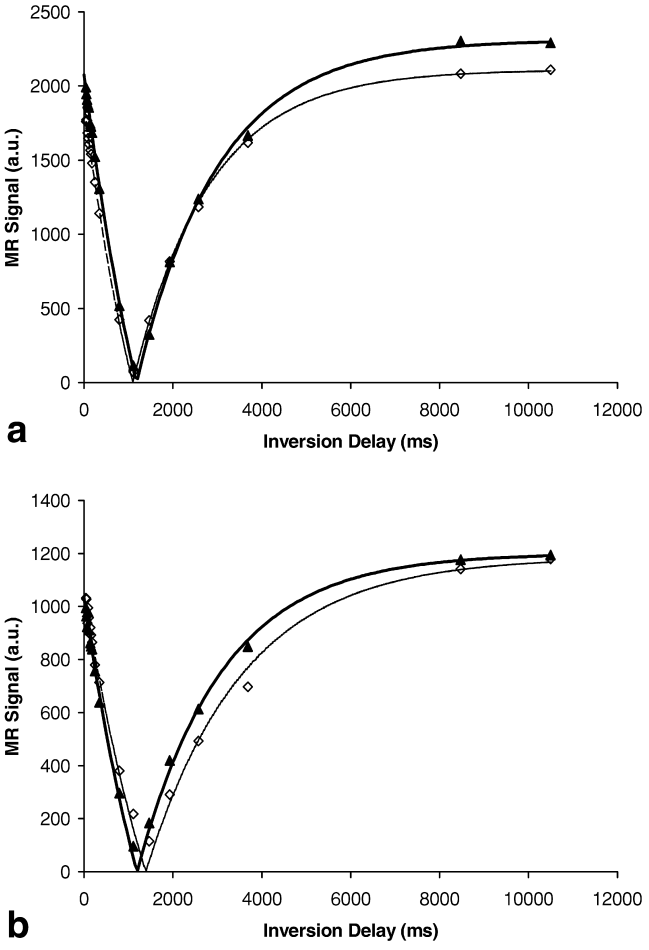

FIG. 6. Inversion recovery time courses of two different voxels from a coronal slice of the rat head at 7 T. Filled triangles and open diamonds represent data acquired before and after, respectively, injection of contrast agent. Lines associated with the triangles and diamonds represent fits performed with Eq. [1], which yield the parameter values presented in Table 1. Note that data and fits are in excellent agreement in all four graphs, both before and after injection.

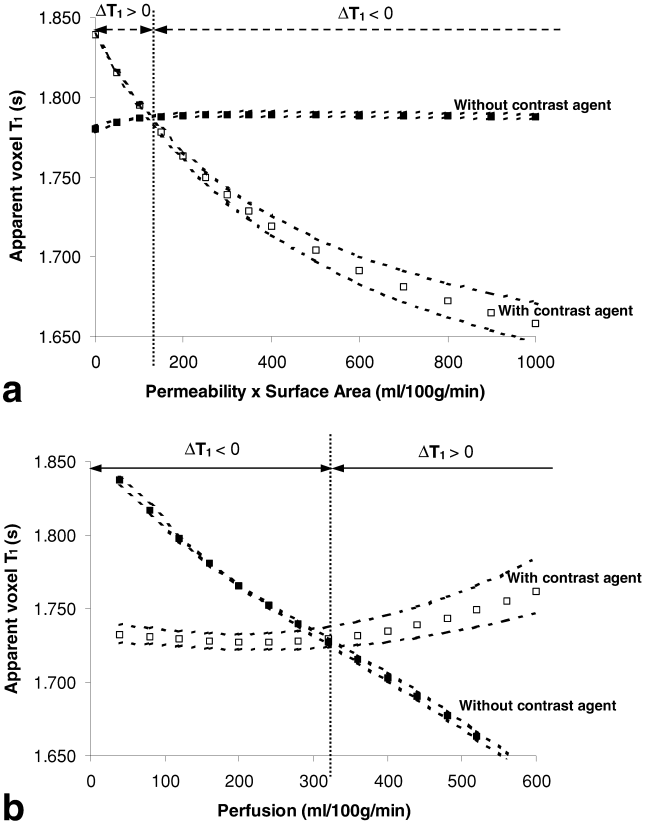

FIG. 7. Apparent voxel T_1 obtained by numerical simulations, before and after injection of a superparamagnetic contrast agent. **a:** Apparent voxel T_1 as a function of the BBB permeability–surface area product to water, for a blood flow of 140 ml / 100 g/min. **b:** Apparent voxel T_1 as a function of blood flow, for PS = 350 ml / 100 g/min. ΔT_1 represents the difference (T_1 after contrast agent – T_1 before contrast agent). Note that ΔT_1 can be either negative or positive. The following parameters were used for the numerical simulations represented in **a** and **b**: T_{1t} = 1.84 sec; T_{1b} = 2.30 sec before contrast agent and T_{1b} = 0.18 sec after contrast agent; V_a:V_c:V_v = 25:40:35. V_b = 3.5@0.5% (i.e., the simulations were conducted three times, for three different blood volume values). Filled squares represent T_1 before contrast agent and open squares T_1 when the contrast agent is present in the vasculature for a total blood volume fraction of 3.5%. The dotted lines represent the voxel T_1 computed for total blood volume fractions of 3% and 4%, so as to indicate the influence of the blood volume fraction on the estimated parameters.

data presented in Fig. 6b ($\Delta T_1 > 0$). For PS product values larger than ~140 ml / 100 g/min, the apparent voxel T_1 decreases after contrast agent injection, which could correspond to the data presented in Fig. 6a ($\Delta T_1 < 0$). In Fig. 7a it can also be seen that, in the absence of contrast agent, the apparent voxel T_1 is also relatively insensitive to the BBB water permeability. After contrast agent injection, there is a clear dependence of the apparent voxel T_1 on the PS product. In Fig. 7a the dotted lines represents the effect on T_1 of a change in the total blood volume fraction used in the simulation (3 or 4% instead of 3.5%). From the width defined by these lines it can be seen that the apparent voxel T_1 is more sensitive to the total blood volume after contrast agent injection.

Table 1
Parameter Values*

	Before injection			After injection		
	Voxel $\mathbf{T}_1$(ms)	$\mathbf{M}^0$ (a.u.)	**C**	Voxel $\mathbf{T}_1$(ms)	$\mathbf{M}^0$ (a.u.)	**C**
Fig. 6a	1839	2313	0.949	1722	2110	0.943
Fig. 6b	1919	1201	0.930	2191	1186	0.942

*Corresponding to the fit by Eq. [1] of the data presented in Fig. 6a and 6b and obtained in the absence and in the presence of contrast agent in the vasculature, from two different voxels located in the rat brain.

Figure 7b shows simulations of the apparent voxel T_1 as a function of blood flow, with PS = 350 ml / 100 g/min (9). As blood flow increases, the apparent voxel T_1 in absence of contrast agent decreases. In the presence of contrast agent, the apparent voxel T_1 is not very sensitive to the value of the blood flow. Note that the quasilinear decay of the apparent voxel T_1 with blood flow is also predicted by the arterial spin-labeling model (11). Finally, Fig. 7b also shows that, depending on blood flow, the change in apparent voxel T_1 induced by the presence of contrast agent in the vasculature can either be positive ($\Delta T_1 > 0$) or negative ($\Delta T_1 < 0$).

Simulations Based on the Physiological Model and Using the Measured Voxel T_1s as a Constraint

Numerical simulations using the physiological model are now performed under the constraint that the simulated voxel T_1s match the measured voxel T_1s, both before and after injection of contrast agent. These constrained simulations yielded an estimation of the BBB permeability to water and of the tissue T_1. Different blood volume fractions for artery, capillary, and vein were used as well as different blood flow values in order to estimate the influence of the choice of the physiological parameters on the outcome of the constrained simulation. The results of this approach are presented in Fig. 8.

Figure 8a shows the values obtained for BBB permeability as a function of the estimated blood flow for a total blood volume fraction of 3.5%. For example, if a blood flow of 140 ml / 100 g/min was assumed, and if V_a:V_c:V_v = 25:40:35 (Fig. 8, black triangles), the simulation of our physiological model under constraint yielded a permeability – surface area product of ~407 ml / 100 g/min and an apparent voxel T_1 of ~1.83 sec (this corresponds to the black lines plotted in Fig. 8a,b). It can be seen that the larger the capillary compartment, the lower the permeability, which is in good agreement with the fact that a constant extraction fraction is required to produced the change in the voxel T_1 that we observed. For example, if all the blood is constrained as being in the capillary (black squares) and assuming a blood flow of 140 ml / 100 g/min, the estimated PS product for the measured voxel T_1 drops to ~320 ml / 100 g/min. On the contrary, when all the blood is constrained to be in the capillary compartment and assuming again a blood flow of 140 ml / 100 g/min, the estimated tissue T_1 slightly increases from 1.83 sec to 1.84 sec (Fig. 8b).

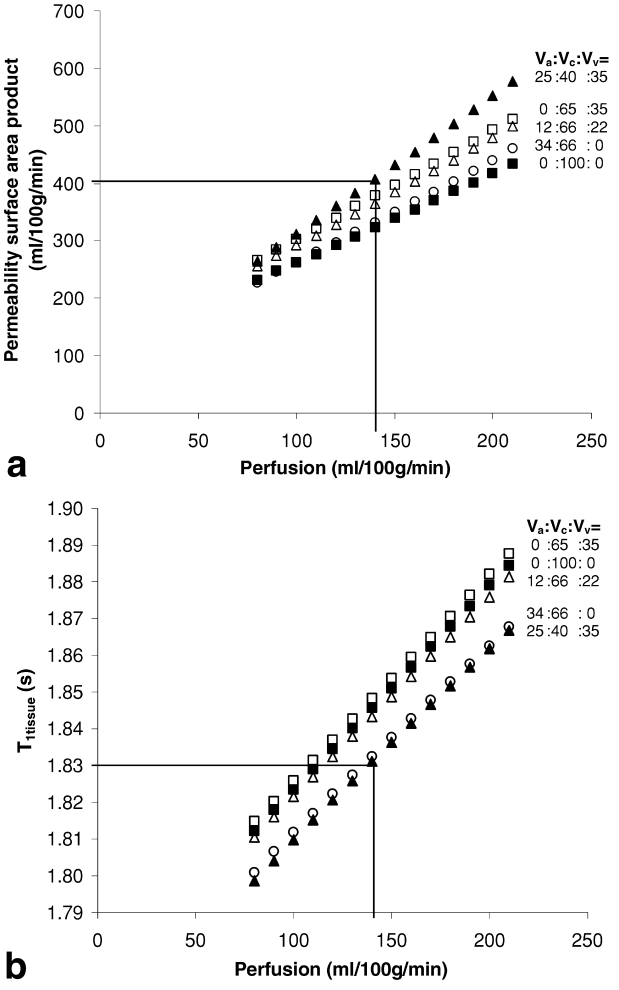

FIG. 8. Constrained simulations of the physiological model: effect of the choice of blood volume fractions and of perfusion. In this figure the model is simulated but with the additional constraint that the predicted voxel T_1s (before and after injection of contrast agent) match the measured T_1s. Different blood volume fractions, as indicated in the captions (respectively, arteriolar, capillary, and venular) have been considered. The black triangles correspond to the choice of fractions used in Fig. 5 (i.e., V_a:V_c:V_v = 25:40:35). The black squares correspond to an entirely exchangeable blood compartment (i.e., V_a:V_c:V_v = 0:100:0), where no arteriolar or venular volume are taken into account. Permeability × Surface Area (**a**) and the tissue T_1 (**b**) are presented as a function of the tissue blood flow, since flow is also an unknown. For example, if the blood flow is 140 ml / 100 g/min and V_a:V_c:V_v = 25:40:35, it can be derived from our data that the Permeability × Surface Area product is 407 ml / 100 g/min and the tissue T_1 was 1.84 sec, as represented by the black lines in **a** and **b**.

DISCUSSION AND CONCLUSION

The characterization of BBB permeability to small molecules, like water, may reveal early changes of the BBB state associated with various pathologies like tumor growth or multiple sclerosis (1–4). To measure BBB permeability to water in vivo a two-point acquisition scheme and a physiological model of analysis are proposed. The comparison of T_1 measurements made at 7 T on the rat brain in the presence and absence of contrast agent in the vasculature demonstrates a small reduction in the apparent voxel T_1 in most of the brain regions except for an increase in the apparent voxel T_1 in a few voxels of the brain. The physiological model, in which blood flow effects are accounted for, yields numerical simulations in good agreement with these observations and could be used to evaluate BBB permeability to water.

Blood Inflow Effects

The increase in apparent voxel T_1 after contrast agent injection was observed in multiple locations in all six animals. Care was taken to accurately measure T_1 (19 TIs

in random order, six averages before contrast agent injection and 17 averages after). Moreover, numerical simulations, which included the effects of blood flow and limited water exchange, demonstrated that the apparent voxel T_1 could increase after the contrast agent was injected. The basis for the observed increase in the apparent voxel T_1 ($\Delta T_1 > 0$) is likely due to a low PS product (Fig. 7a) or a low blood flow (Fig. 7b).

This counterintuitive increase in the apparent voxel T_1 after contrast agent injection is important to consider in detail. Numerical simulations showed that, prior to contrast agent injection and for the case of a spatially selective inversion pulse, the apparent blood longitudinal relaxation occurs faster than the longitudinal relaxation of static blood magnetization (Fig. 3a). The inflow of blood magnetization at equilibrium causes blood magnetization to appear to relax faster than expected from T_1 relaxation alone: with the blood volume and blood flow values used in the numerical simulation, blood flow fills the blood compartment with blood magnetization at equilibrium in about 1.5 sec. This same inflow effect is no longer visible when contrast agent is present in the vasculature (Fig. 3b), since in the presence of contrast agent the true longitudinal relaxation occurs before blood flow has filled the voxel with fully relaxed magnetization. On the contrary, the blood magnetization longitudinal relaxation is slowed by the effect of water exchange between blood and tissue. This effect can be seen in Fig. 2, where, in the capillary compartment, the blood magnetization reduces as the relative volume across the vasculature increases.

The sensitivity of the apparent voxel T_1 to the blood volume fraction is low (Fig. 7.) most certainly because the blood volume represents only a small fraction of the voxel volume. However, in the presence of contrast agent and for high PS product values, i.e., when water molecules in the tissue compartment can access the contrast agent molecules more easily, or for high blood flow values, the sensitivity of the voxel T_1 to the blood volume fraction increases (cf. Fig. 7a, 7b). However, from the analysis of the numerical simulations it appears that blood inflow significantly affects the observed voxel T_1. It can therefore be assessed that the voxel T_1 is mainly sensitive to blood velocity, since small blood volume changes appear to have a minor influence on the voxel T_1 for PS values lower than 400 ml / 100 g/min (cf. Fig. 7a, 7b). This implies that blood flow and blood volume should also be mapped in order to generate accurate PS product maps with the method proposed here.

Computation of the BBB Permeability Surface Area Product

Using our modified version of the Schwarzbauer physiological model, the tissue T_1 and the PS product of the BBB that yield the measured voxel T_1s (in the absence and presence of contrast agent in the vasculature) were estimated using a constrained simulation (see the Results section). Assuming a blood flow of 140 ml / 100 g/min, a total blood volume fraction of 3.5%, and blood volume proportions of V_a:V_c:V_v = 25:40:35, the simulation yielded a tissue T_1 of ~1.83 sec and a PS value of ~407 ml / 100 g/min. According to Crone's equation (26), this permeability yields an extraction fraction of ~95%, which is in good agreement with arterial spin labeling-based measurements in the rat brain under normocapnia (27). The analysis of the influence of the estimated physiological values, chosen as input in these constrained simulations, on the PS product estimation (Fig. 8) shows that, if one assumes that the entire blood compartment exchanges water with the surrounding tissue, the PS product can be underestimated (e.g., compare black square with black triangles in Fig. 8a). If the entire blood compartment is assumed to exchange with the tissue and if blood flow is assumed to be 140 ml / 100 g/min, then the optimization routine generates the same value for the PS product as the one obtained by Schwarzbauer et al. in the brain cortex (331@20 ml / 100 g/min) (9). However, if one used a model in which blood flow effects are not accounted for to analyze the data obtained in this study, it would yield a PS value of ~90 ml / 100 g/min (considering the model proposed by Schwarzbauer et al. and a total blood volume fraction of 3.5%). This underlines the importance of using a model that accounts for blood flow with the experimental scheme proposed here.

In summary, the model proposed here suggests that it is possible to measure the water permeability – surface area product of the BBB by comparing T_1 measurements made in the absence and presence of contrast agent in the vasculature. As this technique only requires two T_1 measurements and a single injection of contrast agent, it is well adapted for clinical studies. Using a spatially selective inversion, the effects of blood flow on the observed T_1 are sizable, as demonstrated using numerical simulations. To determine the PS product with the proposed two-point method it is necessary to know the CBF and CBV. As an initial test of the feasibility of this method, experiments were conducted on a rat model where CBF and CBV are well known. Blood flow could be mapped prior to contrast agent using an arterial spin-labeling technique (28); blood volume could be mapped with a static technique in which the T_2^* reduction induced by the USPIO injection yields the blood volume (15). Finally, since the model used here accounts for blood volumes (exchanging and nonexchanging), blood flow, and BBB permeability, it can also be used to analyze either arterial spin-labeling-based or contrast agent-based measurements, such as the blood volume measurement based on a T_1 change (29).

ACKNOWLEDGMENTS

The authors thank Guerbet Laboratories (Aulnay-sous-Bois, France) for supplying Sinerem® and Chantal Rémy, Emmanuel Fonchy, and Hana Lahrech for stimulating discussions.

APPENDIX

The physiological system, presented in Fig. 1, is fully described by the following parameters:

V_t, tissue volume;
V_a, arterial blood volume;
V_c, capillary (exchanging) blood volume (26,30);
V_v, venous blood volume;

f, blood flow through the voxel;
PS, (blood–brain barrier permeability to water) × (capillary surface area).

One can now define some other characteristics of the system that depend on the previously defined physiological parameters:

$V_b = V_a + V_c + V_v$, total blood volume;
V, volume of a segment within the vasculature, from the voxel entrance ($0 \le V \le V_b$);
$k_t = PS/V_t$, exchange time constant from tissue to blood (capillary);
$k_b = PS/V_c$, exchange time constant from blood (capillary) to tissue.

The relevant associated MR parameters are:

$M_t(V,t)$, tissue magnetization exchanging with blood at volume V and at time t;
M_t^0, equilibrium value of the tissue magnetization;
$M_b(V,t)$, blood magnetization, as a function of V and time;
M_b^0, equilibrium value of the blood magnetization;
T_{1t}, longitudinal relaxation time constant of tissue;
T_{1b}, longitudinal relaxation time constant of blood.

The evolution of magnetization in blood and tissue compartments after an RF pulse is described by:
In arterioles, $0 < V \le V_a$:

$$\frac{\partial \mathbf{M_b}(\mathbf{V},\mathbf{t})}{\partial \mathbf{t}} = \frac{\mathbf{M_b^0} - \mathbf{M_b}(\mathbf{V},\mathbf{t})}{\mathbf{T_{1b}}} - \mathbf{f}\frac{\partial \mathbf{M_b}(\mathbf{V},\mathbf{t})}{\partial \mathbf{V}} \qquad [A1a]$$

In capillaries, $V_a < V \le V_a + V_c$:

$$\frac{\partial \mathbf{M_t}(\mathbf{V},\mathbf{t})}{\partial \mathbf{t}} = \frac{\mathbf{M_t^0} - \mathbf{M_t}(\mathbf{V},\mathbf{t})}{\mathbf{T_{1t}}} + \mathbf{k_b}\mathbf{M_b}(\mathbf{V},\mathbf{t}) - \mathbf{k_t}\mathbf{M_t}(\mathbf{V},\mathbf{t}) \qquad [A1b]$$

$$\frac{\partial \mathbf{M_b}(\mathbf{V},\mathbf{t})}{\partial \mathbf{t}} = \frac{\mathbf{M_b^0} - \mathbf{M_b}(\mathbf{V},\mathbf{t})}{\mathbf{T_{1b}}} - \mathbf{f}\frac{\partial \mathbf{M_b}(\mathbf{V},\mathbf{t})}{\partial \mathbf{V}} - \mathbf{k_b}\mathbf{M_b}(\mathbf{V},\mathbf{t}) + \mathbf{k_t}\mathbf{M_t}(\mathbf{V},\mathbf{t}) \qquad [A1c]$$

In venules, $V_a + V_c < V \le V_a + V_c + V_v$:

$$\frac{\partial \mathbf{M_b}(\mathbf{V},\mathbf{t})}{\partial \mathbf{t}} = \frac{\mathbf{M_b^0} - \mathbf{M_b}(\mathbf{V},\mathbf{t})}{\mathbf{T_{1b}}} - \mathbf{f}\frac{\partial \mathbf{M_b}(\mathbf{V},\mathbf{t})}{\partial \mathbf{V}} \qquad [A1d]$$

where $M_b(0,t)$ is the arterial input function to the voxel. The MR signal arising from the entire voxel (tissue + blood), S(t), can be computed by:

$$\mathbf{S}(\mathbf{t}) = \frac{\mathbf{V_t}}{\mathbf{V_c}}\left[\int_{\mathbf{V_a}}^{\mathbf{V_a}+\mathbf{V_c}} \mathbf{M_t}(\mathbf{V},\mathbf{t})\,\mathbf{dV}\right] + \left[\int_{\mathbf{0}}^{\mathbf{V_b}} \mathbf{M_b}(\mathbf{V},\mathbf{t})\,\mathbf{dV}\right]. \qquad [A2]$$

REFERENCES

1. Tofts PS, Kermode AG. Measurement of the blood-brain barrier permeability and leakage space using dynamic MR imaging. 1. Fundamental concepts. Magn Reson Med 1991;17:357–367.
2. Barbier EL, den Boer JA, Peters AR, Rozeboom AR, Sau J, Bonmartin A. A model of the dual effect of gadopentetate dimeglumine on dynamic brain MR images. J Magn Reson Imag 1999;10:242–253.
3. Doolittle ND, Miner ME, Hall WA, Siegal T, Jerome E, Osztie E, McAllister LD, Bubalo JS, Kraemer DF, Fortin D, Nixon R, Muldoon LL, Neuwelt EA. Safety and efficacy of a multicenter study using intraarterial chemotherapy in conjunction with osmotic opening of the blood-brain barrier for the treatment of patients with malignant brain tumors. Cancer 2000;88:637–647.
4. Barkhof F, van Walderveen M. Characterization of tissue damage in multiple sclerosis by nuclear magnetic resonance. Philos Trans R Soc Lond B Biol Sci 1999;354:1675–1686.
5. Huang ZG, Xue D, Preston E, Karbalai H, Buchan AM. Biphasic opening of the blood-brain barrier following transient focal ischemia: effects of hypothermia. Can J Neurol Sci 1999;26:298–304.
6. Abraham CS, Deli MA, Joo F, Megyeri P, Torpier G. Intracarotid tumor necrosis factor-alpha administration increases the blood-brain barrier permeability in cerebral cortex of the newborn pig: quantitative aspects of double-labelling studies and confocal laser scanning analysis. Neurosci Lett 1996;208:85–88.
7. Wahl M, Whalley ET, Unterberg A, Schilling L, Parsons AA, Baethmann A, Young AR. Vasomotor and permeability effects of bradykinin in the cerebral microcirculation. Immunopharmacology 1996;33:257–263.
8. Cornford EM, Hyman S. Blood-brain barrier permeability to small and large molecules. Adv Drug Deliv Rev 1999;36:145–163.
9. Schwarzbauer C, Morrissey SP, Deichmann R, Hillenbrand C, Syha J, Adolf H, Noth U, Haase A. Quantitative magnetic resonance imaging of capillary water permeability and regional blood volume with an intravascular MR contrast agent. Magn Reson Med 1997;37:769–777.
10. Hamberg LM, Boccalini P, Stranjalis G, Hunter GJ, Huang Z, Halpern E, Weisskoff RM, Moskowitz MA, Rosen BR. Continuous assessment of relative cerebral blood volume in transient ischemia using steady state susceptibility-contrast MRI. Magn Reson Med 1996;35:168–173.
11. Detre JA, Leigh JS, Williams DS, Koretsky AP. Perfusion imaging. Magn Reson Med 1992;23:37–45.
12. Kwong KK, Belliveau JW, Chesler DA, Golberg IE, Weisskoff RM, Poncelet BP, Kennedy DN, Hoppel BE, Cohen MS, Turner R, Cheng H-M, Brady TJ, Rosen BR. Dynamic magnetic resonance imaging of human brain activity during primary sensory stimulation. Proc Natl Acad Sci USA 1992;89:5675–5679.
13. Lee JH, Li X, Sammi MK, Springer CSJ. Using flow relaxography to elucidate flow relaxivity. J Magn Reson 1999;136:102–113.
14. Pawlik G, Rackl A, Bing RJ. Quantitative capillary topography and blood flow in the cerebral cortex of cats: an in vivo microscopic study. Brain Res 1981;208:35–58.
15. Le Duc G, Péoc'h M, Rémy C, Charpy O, Muller RN, Le Bas JF, Décorps M. Use of T_2-weighted susceptibility contrast MRI for mapping the blood volume in the glioma-bearing rat brain. Magn Reson Med 1999;42:754–761.
16. Haase A. Snapshot FLASH MRI. Applications to T_1, T_2, and chemical-shift imaging. Magn Reson Med 1990;13:77–89.
17. Bassingthwaite JB, Goresky CA. Modeling in the analysis of solute and water exchange in the microvasculature. In: Renkin EM, Michel CC, editors. Handbook of physiology. Bethesda, MD: American Physiological Society; 1984. p 549–626.
18. Barbier EL, Silva AC, Kim HJ, Williams DS, Koretsky AP. Perfusion analysis using dynamic arterial spin labeling (DASL). Magn Reson Med 1999;41:299–308.
19. Shockley RP, LaManna JC. Determination of rat cerebral cortical blood volume changes by capillary mean transit time analysis during hypoxia, hypercapnia and hyperventilation. Brain Res 1988;454:170–178.
20. Meier P, Zierler KL. On the theory of the indicator-dilution method for measurement of blood flow and volume. J Appl Physiol 1954;6:731–744.
21. Neil JJ, Song SK, Ackerman JJ. Concurrent quantification of tissue metabolism and blood flow via 2H/31P NMR in vivo. II. Validation of the deuterium NMR washout method for measuring organ perfusion. Magn Reson Med 1992;25:56–66.
22. Van Zijl PC, Eleff SM, Ulatowski JA, Oja JM, Ulug AM, Traystman RJ, Kauppinen RA. Quantitative assessment of blood flow, blood volume and blood oxygenation effects in functional magnetic resonance imaging. Nat Med 1998;4:159–167.

23. Brooks RA, Brunetti A, Alger JR, Di Chiro G. On the origin of paramagnetic inhomogeneity effects in blood. Magn Reson Med 1989;12:241–248.
24. Ogawa S, Lee TM, Kay AR, Tank DW. Brain magnetic resonance imaging with contrast dependent on blood oxygenation. Proc Natl Acad Sci USA 1990;87:9868–9872.
25. Ogawa S, Lee TM, Nayak AS, Glynn P. Oxygenation-sensitive contrast in magnetic resonance image of rodent brain at high magnetic fields. Magn Reson Med 1990;14:68–78.
26. Crone C. The permeability of capillaries in various organs as determined by use of the 'indicator diffusion' method. Acta Physiol Scand 1963;58:292–305.
27. Silva AC, Zhang W, Williams DS, Koretsky AP. Estimation of water extraction fractions in rat brain using magnetic resonance measurement of perfusion with arterial spin labeling. Magn Reson Med 1997;38:35–58.
28. Calamante F, Thomas DL, Pell GS, Wiersma J, Turner R. Measuring cerebral blood flow using magnetic resonance imaging techniques. J Cereb Blood Flow Metab 1999;19:701–735.
29. Lin W, Paczynski RP, Kuppusamy K, Hsu CY, Haacke EM. Quantitative measurements of regional cerebral blood volume using MRI in rats: effects of arterial carbon dioxide tension and mannitol. Magn Reson Med 1997;38:420–428.
30. Eichling JO, Raichle ME, Grubb RLJ, Ter-Pogossian MM. Evidence of the limitations of water as a freely diffusible tracer in brain of the rhesus monkey. Circ Res 1974;35:358–364.